Solar Semidiurnal Tides in the Troposphere: Detection by Radar Profilers

C. David Whiteman and Xindi Bian
Pacific Northwest Laboratory, Richland, Washington

ABSTRACT

A short review of solar semidiurnal atmospheric tides is presented. Semidiurnal atmospheric tides have been documented in the troposphere primarily through analyses of long time series of surface pressure measurements, although the winds produced by these tides have, by now, been well documented in the middle and upper atmosphere. Recent research using UHF and very-high-frequency radar wind profilers has now identified tidal wind perturbations in tropospheric data. This review focuses on the tidal wind characteristics and the distinctive signature of this wind system in radar profiler data analyses.

1. Introduction

As UHF and very-high-frequency (VHF) radar wind profilers have become more widely available, it has become possible to routinely detect and monitor the influence of solar semidiurnal tides on the earth's troposphere. The tidal influences on the middle and upper atmosphere have been well documented and modeled by geophysicists, but many meteorologists who have worked solely on tropospheric problems are unfamiliar with the solar semidiurnal tides. This paper provides a short review of this atmospheric tidal phenomenon, pointing out the physical causes of the tides, their influence on the earth's atmosphere, and the distinctive characteristics of the tropospheric tides in radar profiler data analyses.

Several earlier reviews of solar tides are available for the interested reader. The book by Chapman and Lindzen (1970) provides an excellent broad overview of scientific research on solar and lunar atmospheric tides up to the late 1960s. A review by Lindzen (1979) updated the Chapman and Lindzen book by concentrating on new observations and theoretical developments. More recently, Lindzen (1990) has provided an interesting historical summary of research on the tides, emphasizing the scientific hypotheses that were tested, the incremental progress made in understanding the tides, and the applications and pitfalls of the scientific method in tidal investigations. In the years since the Chapman and Lindzen book was published, there has been a great deal of activity in modeling the tides with upper-atmospheric and global climate models (e.g., Lindzen and Hong 1974; Walterscheid and DeVore 1981; Forbes 1982; Hamilton 1984; Zwiers and Hamilton 1986; Forbes and Hagan 1988). We will not review this modeling literature here. Readers of literature on the upper atmosphere are cautioned that coordinate systems, symbols, and other aspects of the upper-atmospheric work use mathematical conventions that frequently differ from those in common use in the troposphere.

2. Review of solar semidiurnal tides

The term "solar semidiurnal tide" has been applied to the small, regular, atmospheric pressure oscillations that occur with a period of half a solar day (i.e., 12 hours). Such pressure oscillations are a well-known feature of the surface pressure climatology and

Corresponding author address: Dr. C. David Whiteman, Battelle Northwest Laboratories, P.O. Box 999, Richland, WA 99352.
e-mail: cd_whiteman@pnl.gov
In final form 28 August 1995.

have been observed over the earth's surface since Toricelli's invention of the barometer in about 1643. The semidiurnal surface pressure oscillations have typical amplitudes of 1.2 hPa at the equator and vary from 0.9 hPa at the southern border of the United States to 0.3 hPa at the Canadian border (U.S. Weather Bureau 1943). It was recognized very early that the amplitudes of the semidiurnal pressure perturbations decrease with increasing latitude and that the semidiurnal signal is more easily detected in quiescent tropical barometric records than in midlatitude records, where the small signal can be masked by traveling synoptic-scale pressure disturbances. The semidiurnal pressure oscillations are well known by weather forecasters because measured pressure tendencies must be corrected for these regular oscillations if the pressure tendency field is expected to be representative of the synoptic-scale pressure systems associated with traveling weather disturbances.

The interpretation of the surface pressure oscillation as a solar tide has a long historical basis and comes from the characteristics of the oscillation, which are in some respects similar to the characteristics of ocean tides. In the case of ocean tides, two high tides and two low tides occur each day at a given location, with the high tide generally occurring at the time of the overhead transit of the moon. The ocean tides are produced primarily by the gravitational attraction of the moon, although the gravitational attraction of the sun produces an important secondary effect, causing the strength and period of the tide to vary somewhat. Because of unbalanced forces on the earth's surface, the fluid envelope is deepest directly under the moon, where the gravitational attraction is greatest, and on the opposite side of the earth, producing in a single period of rotation two tides per day at a given longitude. Because the ocean tides follow the motion of the moon around the earth, they have a lunar periodicity, and because the lunar period differs from the 24-h solar period on which our time system is based, the times of high tide vary from day to day. The atmosphere, like the oceans, is free to move in response to the gravitational attraction of the moon, so that a similar lunar tide in the earth's atmosphere can also be expected. Such atmospheric gravitational tides were predicted by Newton (1687) in his *Principia Mathematica,* and he correctly surmised that lunar tidal effects on the earth's atmosphere would be very small. Experimental confirmation of the existence of lunar gravitational tides was provided by Chapman (1918) after an extensive effort, dealing with 64 years of hourly surface pressure data from Greenwich, England. Lunar tidal amplitudes vary strongly with latitude and are generally in the range from 0.005 to 0.080 hPa (Haurwitz and Cowley 1970).

The semidiurnal surface pressure oscillations are similar to the ocean tides in having two maxima and two minima per day, but their periodicity is an exact harmonic of the solar period, and at a given station on the earth, the maxima and minima occur every day at about the same local mean solar time. The pressure perturbation pattern, having two waves around the earth, follows the apparent motion of the sun from east to west and so must have a solar rather than a lunar or gravitational origin. The time of pressure maximum represents the time when column mass is at a maximum, but unlike in the case of the lunar tide, this does not occur at the time of the transit of the heavenly body (in this case, the sun). Rather, the two daily maxima occur about 2.3 h before solar noon and before solar midnight.

Since the semidiurnal tides have a clearly solar, rather than lunar or gravitational, origin, Laplace (1825) hypothesized that they were produced by the thermal effects of the sun. However, this immediately raised the question of why the tidal response of the earth's atmosphere was predominantly semidiurnal rather than diurnal, since the main solar thermal forcing is diurnal. It was easy to understand how diurnal circulations could be generated between the sunny and shaded sides of the earth and how such circulations would follow the apparent path of the sun. But why would the semidiurnal signal be so strong relative to the diurnal tidal signal? A possible answer to this paradox, suggested by Kelvin (1882) and investigated in the early part of the century, was that a small semidiurnal signal could be amplified by resonance in the earth's atmosphere. An especially interesting account of the 70-year-long scientific pursuit of this flawed hypothesis, which was ultimately proven to be incorrect, has been provided by Lindzen (1990).

A partial answer to the paradox came from two papers published in the 1960s. A paper published by Siebert (1961) showed that a semidiurnal thermal signal could be produced by the absorption of solar radiation by water vapor in the earth's atmosphere. According to his calculations, this heating could account for approximately one-third of the semidiurnal tidal amplitude. A later paper by Butler and Small (1963) showed that most of the remaining two-thirds of the observed semidiurnal amplitudes could be explained in a like manner by solar absorption by ozone

in the upper stratosphere. A further answer to the paradox was provided by Lindzen (1967), who showed that the diurnal signal aloft is unable to propagate vertically downward to the surface at latitudes poleward of 30°N and 30°S because the local pendulum day at these latitudes is less than 24 h. Furthermore, vertically propagating waves at latitudes equatorward of 30°N and 30°S are of short vertical wavelength and are subject to destructive interference effects. Thus, the relative sizes of the diurnal and semidiurnal signals in the troposphere are affected not only by the production of a semidiurnal signal by ozone and water vapor absorption but also by a wave propagation process that produces weaker diurnal signals than expected.

Because surface pressure is a measure of the weight of the air column above a site, the westward traveling surface pressure perturbations represent daily changes of air mass redistribution in the atmosphere of about 0.1% (1-hPa oscillations at a sea level pressure of about 1000 hPa), and the redistribution is accomplished by wind systems that sweep across the global atmosphere following the sun's apparent movement. The existence of the pressure gradients associated with the traveling semidiurnal pressure perturbations at the surface and their extension upward into the earth's atmosphere imply that tidal *wind* oscillations will also occur. In fact, such winds are a well-known and rather prominent feature of the middle and upper atmosphere, especially in the ionosphere, where the semidiurnal winds produce strong geomagnetic effects.

Internal gravity waves excited by the solar heating in the upper stratosphere propagate upward and downward through the earth's atmosphere. The upward propagation and increasing amplitude of these waves with height results in the semidiurnal tidal wind oscillations in the mesosphere and lower thermosphere, with amplitudes reaching 20 m s^{-1}, that were identified by geophysicists in the 1950s (Greenhow and Neufeld 1961). The gravity waves are damped as they propagate downward into the troposphere. Thus, despite the regularity of the pressure signal at the ground, analyses of surface anemometer data have been largely unsuccessful in identifying semidiurnal tidal wind oscillations at the earth's surface. This is thought to be caused by the small magnitude of the tidally produced surface pressure gradients relative to the pressure gradients associated with traveling storms, as well as by the effects of friction and flow obstacles in the earth's boundary layer. In addition, diurnal circulations are present at most surface locations, and the formal fitting of Fourier components to time-asymmetric diurnal wind circulations produced by the nonequal lengths of the day/night periods can produce spurious higher frequency components that obscure the true solar semidiurnal signal near the surface. Thus, attempts to isolate the semidiurnal wind signal (e.g., Haurwitz and Cowley 1969; Chapman 1951) have not produced a tidal signal matching the theoretically predicted phases and amplitudes.

The first investigation of midlatitude tropospheric semidiurnal tidal winds was conducted by Wallace and Tadd (1974). Their clever investigation technique used data from a period when rawinsondes were launched four times per day, and they inferred semidiurnal tidal characteristics from differences in 6-h rawinsonde wind observations by assuming that the semidiurnal wind vector rotates in a roughly circular pattern over the course of a day. Their investigation provided important information on the semidiurnal tidal wind system in the troposphere, although it suffered from a rather short dataset, a lack of volume- or time-averaged wind observations, decreasing accuracy of the wind observations with height, and the impossibility of separating the semidiurnal oscillations from higher-frequency harmonics.

With the advent of continuously operating, vertically pointing radar wind profilers, however, new measurement tools have become available that can continuously monitor winds above the surface layer and through the depth of the troposphere. Data from radar wind profilers, in contrast to rawinsondes, are integrated over fixed atmospheric volumes and times, have an acceptable range and accuracy for tropospheric investigations, and have a much better temporal resolution [wind data samples in the National Oceanic and Atmospheric Administration's (NOAA's) Wind Profiler Demonstration Network are collected at 6-min intervals], allowing the separation of semidiurnal and higher frequency signals. Further, the availability of 915-, 404-, and 50-MHz radars allows one to investigate wind systems over different vertical ranges and resolutions, and the quantity and spatial coverage of such data are rapidly increasing.

The first investigation of solar semidiurnal tides using radar profilers was apparently made by Williams et al. (1992) for the east–west component of the semidiurnal wind at Christmas Island, a site near the equator. The north–south component was not reported, as it becomes small to the point of vanishing as the equator is approached. In this investigation, four

years of 50-MHz radar profiler data were used to detect east–west tidal amplitudes of about 0.2 m s^{-1} through the depth of the troposphere.

Our recent analyses of 404- and 915-MHz radar wind profiler data at midlatitude sites in the United States (Whiteman and Bian 1994, 1995) have identified coherent semidiurnal wind oscillations that are a significant feature of the tropospheric wind climatology above the frictional boundary layer. Our interpretation that these wind oscillations are semidiurnal atmospheric tides is based on the correspondence between their observed characteristics and the characteristics of semidiurnal tides predicted by dynamic models of the earth's atmosphere. In the following sections, we will use a simple dynamical model to illustrate predicted tidal characteristics and will then summarize the radar wind profiler data analyses.

3. A simple dynamic model of semidiurnal solar tides

The general global characteristics of tidal pressure and wind oscillations can be illustrated with a simple atmospheric dynamical model, which can be driven by observations of the semidiurnal surface pressure perturbation.

The general global characteristics of the semidiurnal tidal surface pressure perturbation are provided by Haurwitz's (1956) smoothed mathematical fit to semidiurnal surface pressure perturbations obtained from a harmonic analysis of data from 296 global barometric stations:

$$p = p_s \cos^3\phi \sin\left[2(t' + \lambda) + \eta_0\right] \text{ hPa}, \qquad (1)$$

where p_s is 1.16 hPa, ϕ is latitude, t' is UTC reckoned in angle at the rate of 360° per mean solar day from lower transit (i.e., midnight), λ is east longitude, and η_0 is 158°. The global pressure perturbation field from this formula at 0000 UTC is plotted in Fig. 1. The maximum amplitudes of the semidiurnal pressure oscillation occur at the equator, with two complete pressure waves surrounding the earth. The waves move from east to west following the apparent path of the sun, with pressure maxima occurring at $t = t' + \lambda = (90° - \eta_0)/2$ or 0944 and 2144 local mean solar time (LMST) at all longitudes.

The characteristics of the tidal wind oscillations produced by the semidiurnal pressure oscillations can be determined from the equations of motion by following a method developed by Chapman and Lindzen (1970), which treats the semidiurnal pressure wave as a small perturbation on an undisturbed background state. The perturbation equations for atmospheric motion above the frictional boundary layer on a rotating spherical earth can then be written as

$$\frac{\partial u}{\partial t} - 2\Omega v \sin\phi = -\frac{1}{\rho R_E \cos\phi}\frac{\partial p}{\partial \lambda},$$

$$\frac{\partial v}{\partial t} + 2\Omega u \sin\phi = -\frac{1}{\rho R_E}\frac{\partial p}{\partial \phi}, \qquad (2)$$

where u and v denote, respectively, the eastward and northward semidiurnal wind components, Ω is the angular velocity of the earth, ρ is air density, R_E is the earth's radius, and p is the semidiurnal tidal pressure perturbation. In this equation, the nonlinear advection terms are neglected because they are quite small (Haurwitz 1962). Equation (1) provides a simple analytical function for the semidiurnal perturbation of surface pressure as a function of latitude and longitude, which can be used to determine the pressure gradients on the rhs of (2). The resulting solution should be indicative of winds in the free atmosphere at the top of the frictional boundary layer. Differentiating (1) with respect to latitude and longitude, substituting into (2), and expressing the time derivative in terms of its longitudinal equivalent, $\partial/\partial t = 2\Omega(\partial/\partial\lambda)$, we obtain Chapman and Lindzen's (1970) solutions for the semidiurnal wind components:

$$u = C_s\left(1 + 1.5\sin^2\phi\right)\sin\left(2t + \eta_0 + 180°\right),$$

$$v = -2.5C_s \sin\phi \sin\left(2t + \eta_0 + 90°\right), \qquad (3)$$

where $C_s = p_s/\rho R_E\Omega \cong 0.2$ m s^{-1} and t is LMST.

The u and v components are, respectively, 180° and 90° out of phase with the pressure oscillation (Fig. 2). The two wind components are in quadrature and are of approximately equal amplitude poleward of 20°N in both hemispheres, so that the wind vector $\mathbf{V} = u\mathbf{i} + v\mathbf{j}$ should rotate clockwise on a near-circular path twice per day. From (1), the pressure perturbation decreases with latitude, but because the merid-

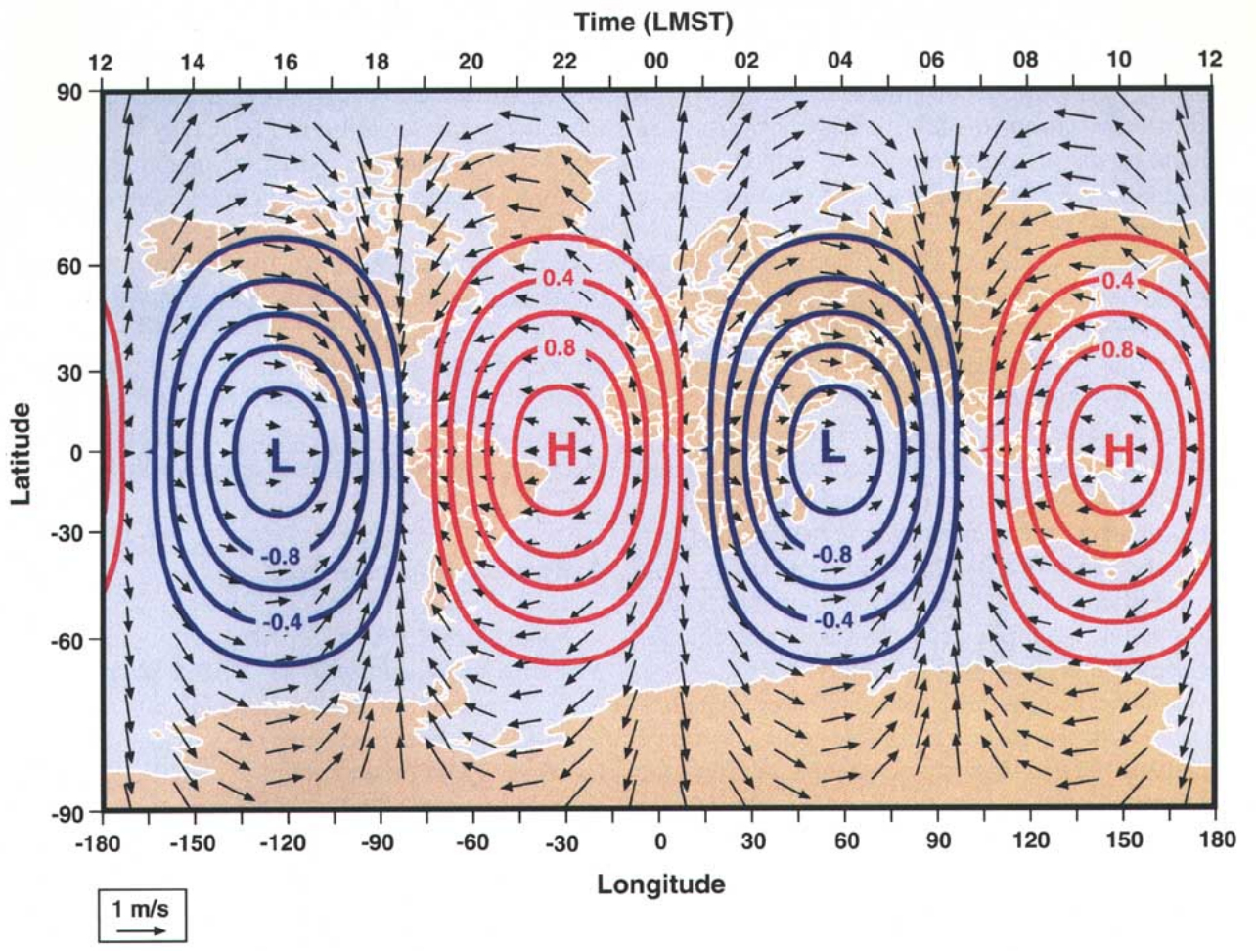

FIG. 1. Equinoctial semidiurnal tidal pressure and wind perturbation patterns on the earth's surface at 0000 UTC. Pressure perturbations are shown in hPa. The scale at the top of the figure represents the local mean solar times corresponding to the longitudes on the bottom scale at 0000 UTC. Because the pressure and wind patterns follow the sun's apparent movement, the patterns travel from east to west and appear at all longitudes at the time indicated on the upper scale.

ians converge toward the poles and decrease the actual distance between the wave crests, the pressure gradient remains sufficient to produce tidal winds. Because (1) and (3) are simple functions of latitude and longitude (or, equivalently, time), the wind patterns that accompany the pressure perturbations can be plotted on a map of the earth at a given time. This is done in Fig. 1 for 0000 UTC. A low and high pressure perturbation on the dark side of the earth are opposite the centers of low and high pressure perturbation on the sunny side of the earth. Westerly wind perturbations occur over the low pressure areas in both hemispheres, and easterly winds occur over the high pressure areas. At the equator, the winds have no v component. The east wind component maxima are attained at 0344 and 1544 LMST in both hemispheres. The north wind component maxima are attained at 0044 and 1244 LMST in the Northern Hemisphere but at 0644 and 1844 in the Southern Hemisphere. The winds converge along a given meridian about 44 min after sunrise and sunset and di-

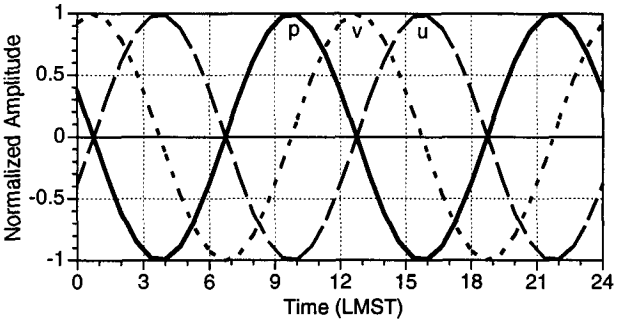

FIG. 2. Phase relationships between pressure and the u and v wind components, using Haurwitz's (1956) equation for the global semidiurnal surface pressure and Chapman and Lindzen's (1970) solution to the momentum equations.

verge over the same meridian 44 min after midday and midnight. These divergences (maximum $\sim 6 \times 10^{-7}$ s^{-1}) are generally small, relative to typical midlatitude synoptic-scale divergences, but are thought by some investigators to be responsible for the semidiurnal precipitation maxima that have been observed in the Tropics and subtropics (Wallace 1975; Brier and Simpson 1969). Lindzen (1978) and Hamilton (1981, 1983) have provided an interesting alternative interpretation of the relationship between semidiurnal precipitation maxima and solar tides. They have suggested that the precipitation maxima are not produced by the tidal pressure and/or wind perturbations, but instead, that the latent heat release associated with the precipitation maxima provides a semidiurnal source of tropospheric heating that will affect the phase of the tidal wind oscillations. This interpretation, however, leaves an important question unanswered. What physical effect is responsible for the semidiurnal precipitation signal?

While the patterns and relationships between pressure and wind are as shown in Figs. 1 and 2, it should be emphasized that Haurwitz's equation, on which the pressure and wind patterns are based, was determined as a smoothed fit to semidiurnal pressure data at a number of surface stations over the globe, as interpolated to a 10°–15° latitude–longitude grid. The fit of (1), while adequately representing the pressure pattern over much of the globe, is inaccurate in the vicinity of major mountain barriers and loses accuracy as the poles are approached. Haurwitz (1956) remarked on this and even presented an expanded equation providing a better fit in the polar regions, where, as previous investigators discovered, a standing pressure wave occurs. Spar (1952) used pressure data from 100 U.S. weather stations (U.S. Weather Bureau 1943) to provide a more detailed representation of pressure perturbation patterns over the conterminous United States, where anomalous amplitude and phase isoline patterns were apparent over and west of the Rocky Mountains and Appalachians. Similar looking tidal oscillations had been produced by Kertz's (1951) model of the effect of a hypothetical north–south ridge on the propagation of semidiurnal tides, and Wallace and Hartranft (1969) found similar topographic anomalies when investigating diurnal tides. More recently, Davies and Phillips (1985) found asymmetries in the diurnal and semidiurnal pressure fields in a north–south cross section across the Alps, and Frei (1994) and Frei and Davies (1993) have developed hypotheses regarding the origin of this mountain-bound pressure anomaly and its influence on mountain drag and momentum transport. Thus, mountain-modified tides that are not shown explicitly in the smoothed representation in Fig. 1 may have important effects on mountain drag, momentum transport, tidal convergence fields, and perhaps even on precipitation fields.

While surface pressure observations have been available for many years, only in recent years have long-term data from remote sensing systems been available to search directly for the semidiurnal tropospheric tidal winds having the characteristics predicted above. The radars that can be used to observe semidiurnal tidal winds in the lower troposphere are discussed below.

4. Radar wind profilers

Pulsed Doppler clear-air radar wind profilers are now in widespread use in the United States, having been developed for meteorological applications by NOAAs Environmental Technology Laboratory (then, the Wave Propagation Laboratory) in the 1980s. Radar profilers in the United States presently operate on three frequencies: 915, 404, and 50 MHz. These wind profilers and their operating characteristics have been described by Doviak and Zrnic (1993) and Neff (1990). Radar profiler data processing procedures have been described by Strauch et al. (1984). These radar profilers detect signals backscattered from turbulence-induced refractive index variations with a scale of half the radar wavelength. As the refractive index irregularities drift with the mean wind, their translational velocity provides a direct measure of the mean wind vector. The lower-frequency profilers probe deeper into the atmosphere and overcome the vertical range limitations of the higher-frequency profilers, although they provide a somewhat poorer range resolution. The 404-MHz profilers have a maximum range of 16 km, while the 50-MHz profilers, under idealized conditions, can attain a range of 20 km (Doviak and Zrnic 1993). In our experience, however, the typical range is closer to half of these idealized values.

5. Analysis of radar wind profiler data

To illustrate the use of radar profiler data for observing tropospheric tides, we use hourly wind profiles at the four U.S. stations shown in Fig. 3 and described in Table 1. The sites were chosen to illus-

trate tidal characteristics in midlatitudes over a broad range of longitude. The data used in this paper are 1-h-average vertical profiles of horizontal winds from continuously operating, unattended, three-beam 915- and 404-MHz radar wind profilers operated in the low vertical resolution mode. The 915-MHz data come from a portable radar profiler operated by NOAA at Temple Bar, Arizona, during the MOHAVE experiment. The 404-MHz data come from NOAA's Wind Profiler Demonstration Network, an operational network of radar profilers located primarily in the central United States. Data from the 915-MHz profiler are hourly averages over 103-m-deep altitude intervals beginning with the layer centered at 177 m above ground level (AGL); data from the 404-MHz profilers are hourly averages over 250-m altitude intervals beginning with the layer centered at 500 m AGL. Because radar beam scattering from migrating birds is known to contaminate radar profiler wind data (Wilczak et al. 1995), we have focused our analyses entirely on the winter season when migrations are at a minimum.

TABLE 1. Site locations and periods of record.

Site	ID	Latitude (°N)	Longitude (°W)	Elevation (m MSL)	Period of record
NOAA Wind Profiler Demonstration Network (404 MHz)					
Hudson, MA	HUD	42.41	71.48	93	JFD 91 and JFD 92
Haviland, KS	HAV	37.65	99.09	648	JFD 91 and JFD 92
Platteville, CO	PLT	40.18	104.72	1524	JFD 91 and JFD 92
Project MOHAVE (915 MHz)					
Temple Bar, AZ	TBR	36.02	114.33	460	3 Jan–19 Apr 1992

The basic wind dataset at each site is composed of the time series of hourly wind vectors at each altitude segment or "range gate" for the entire period of record. For each site, a mean climatological wind day was determined as illustrated for Temple Bar in Fig. 4, where each of the vectors (i.e., for each range gate and hour of the day) was determined by vector averaging all available winds for that hour and range gate for the entire period of record. The semidiurnal wind oscillation was then isolated by performing harmonic analyses (Stull 1988) on the eastward directed (u) and northward directed (v) components of the 24 vector winds in the mean climatological wind day at each range gate. Because signal-to-noise ratios decrease

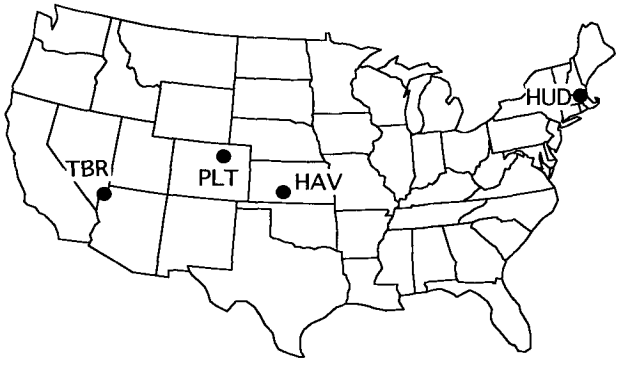

FIG. 3. Radar profiler locations.

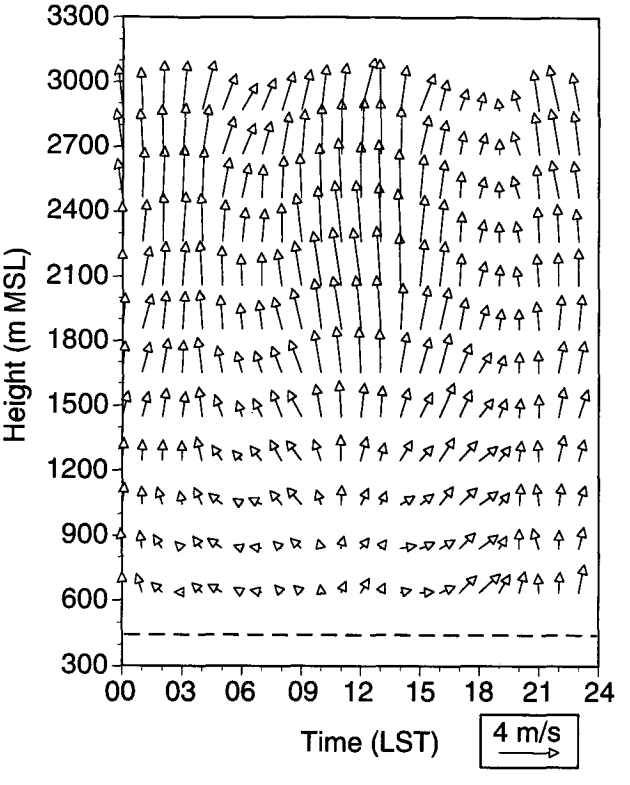

FIG. 4. Mean daily time–height cross section of horizontal vector winds at Temple Bar, Arizona. Times are in local standard time. Vectors pointing to the right are blowing from the west, vectors pointing up are blowing from the south, etc. The dashed line indicates surface elevation.

with radar range and a "consensus" algorithm requires consistent multiple wind determinations on each beam before a valid hourly wind can be reported, the number of reported hourly winds going into the vector average decreases with height, as shown in Fig. 5, reducing the statistical significance of data from the upper altitudes. Radar range can also vary with the time of day and atmospheric conditions, although this variation was small for the wintertime data used (Fig. 6).

In harmonic analysis, the discrete data points in a time series are fit by a series of sine and cosine terms to determine the amplitudes and phases of the harmonic terms. In the case of a discrete time series with a finite number of points, only a finite number of sine and cosine terms are required to fit the points exactly. For a total of N data points in a period T, the highest frequency waves that can be resolved by discrete Fourier transforms are $N/2$ waves. In our analyses, T is 24 h, and the number of points N is 24, so that 12 (i.e., $N/2$) harmonic components with frequencies between 1 and 12 waves per day can fit the 24-h points exactly, such that

$$u(t'') = u_0 + \sum_{n=1}^{N/2}\left(a_n \cos nt'' + b_n \sin nt''\right) = u_0 + \sum_{n=1}^{N/2} A_{un} \sin\left(nt'' + \eta_{un}\right),$$

$$v(t'') = v_0 + \sum_{n=1}^{N/2}\left(c_n \cos nt'' + d_n \sin nt''\right) = v_0 + \sum_{n=1}^{N/2} A_{vn} \sin\left(nt'' + \eta_{vn}\right), \quad (4)$$

where t'' is LST, u_0 and v_0 are the daily mean wind components, A_{un} and A_{vn} are the amplitudes, and η_{un} and η_{vn} are the initial phases of the nth harmonic terms for u and v.

The harmonic terms have their maxima at times $t''_{un} = (90° - \eta_{un})/n$ and $t''_{vn} = (90° - \eta_{vn})/n$ and at intervals $360°/n$ thereafter throughout the day. For comparison of times between sites and with theoretical calculations, it is useful to convert the local standard times in which the data are recorded into LMST using the formula $t_n = t''_n + (\lambda_0 - \lambda)/15$, where λ_0 is the standard meridian for the time zone. Given the phases of the u and v components, the direction of rotation of the wind vector is counterclockwise if $\sin(\eta_{un} - \eta_{vn})$ is positive and clockwise if $\sin(\eta_{un} - \eta_{vn})$ is negative (Haurwitz 1962).

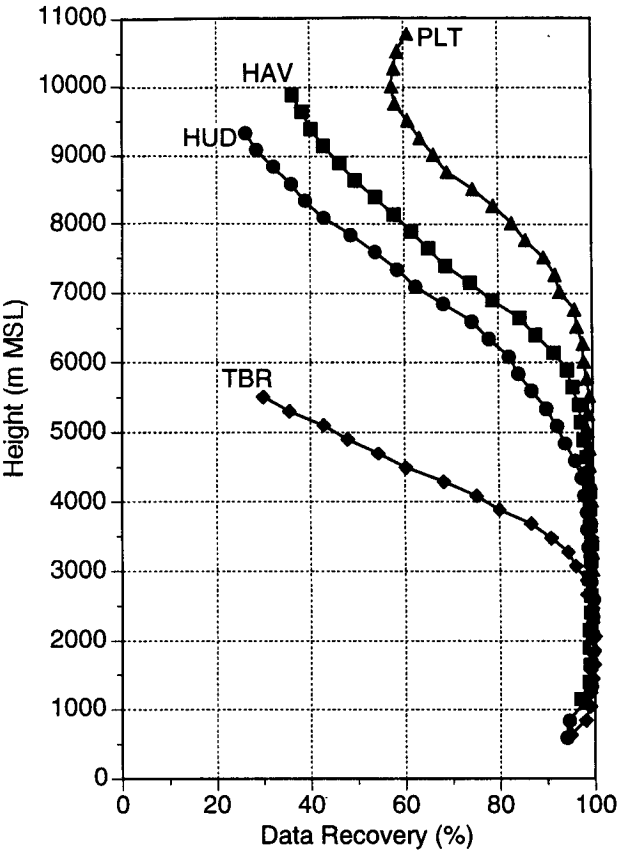

FIG. 5. Percentage of valid wind measurements as a function of height. The number of possible hourly wind profiles is 2451 at HAV, 2798 at HUD, and 2486 at PLT, and 1783 at TBR.

In time series analyses we frequently wish to determine how much of the variance of a time series is associated with a particular harmonic term, without regard to the precise phase of the wave. A measure of the variance of the hourly wind vectors $\mathbf{V}_j$ can be expressed by considering the variances of the components u_j and v_j, which are given by

$$\sigma_u^2 = \frac{1}{N}\sum_{j=1}^{N}\left(u_j - u_0\right)^2, \qquad \sigma_v^2 = \frac{1}{N}\sum_{j=1}^{N}\left(v_j - v_0\right)^2. \quad (5)$$

Alternatively, the variances can be calculated from the coefficients of the Fourier series, such that

$$\sigma_u^2 = \sum_{n=1}^{N/2}\left[(a_n)^2 + (b_n)^2\right] = \sum_{n=1}^{N/2}(A_{un})^2,$$

$$\sigma_v^2 = \sum_{n=1}^{N/2}\left[(c_n)^2 + (d_n)^2\right] = \sum_{n=1}^{N/2}(A_{vn})^2. \quad (6)$$

The sum of the variances of the u and v components is an estimate of the variance of the vector wind field and is given by

$$\sigma_u^2 + \sigma_v^2 = \sum_{n=1}^{N/2}\left[(a_n)^2 + (b_n)^2 + (c_n)^2 + (d_n)^2\right] = \sum_{n=1}^{N/2}\left[(A_{un})^2 + (A_{vn})^2\right]. \quad (7)$$

Thus, we can interpret $P_n = [(A_{un})^2 + (A_{vn})^2]/(\sigma_u^2 + \sigma_v^2)$ as the portion of the variance of the vector wind field explained by the nth harmonic.

Table 2 provides an example of harmonic analysis results for Platteville, Colorado. In this table and in the figures that follow, data are listed and plotted only to altitudes where data recovery remained above 75%. This level was 6898 m MSL at HAV, 6343 m at HUD, 8274 m at PLT, and 4088 m at TBR. Table 2 provides information for each of the range gates on the daily mean vector wind components (u_0 and v_0), the diurnal and semidiurnal harmonics (amplitudes and phases for each component), and the normalized power density of the diurnal and semidiurnal harmonics. Several conclusions can be drawn from the table. First, the normalized diurnal and semidiurnal power densities add up to 90% or more through much of the sounding depth, with the exception of the first four range gates, where friction effects are important, and at the upper levels of the sounding, where the data become noisier. This shows that the daily course of the winds at various altitudes can be reasonably well approximated by the sum of the mean daily wind and the first two harmonics and that the terdiurnal (n = 3) and higher-frequency harmonics (n = 4–12) play only a small role in explaining the variance of the winds. Second, the power density of the semidiurnal harmonic increases with height, becoming more important than the diurnal component above about 4500 m MSL. This height is somewhat above the mean crest height of the Rocky Mountains to the west of Platteville. Third, except near the surface where the diurnal winds are strong, the diurnal and semidiurnal harmonics have generally comparable amplitudes. Fourth, in contrast to the behavior of the diurnal components, the phase of the semidiurnal harmonic components, shown here as the times of the wind maxima, varies only weakly with height above the first four range gates. In rough agreement with theory, which calls for the v-component maximum to occur at 0044 or 0.74 h LMST, the v-component maximum occurs between 0.3 and 1.2 h LMST. Finally, the v component for the semidiurnal harmonic leads the u component by about 3 h (i.e., 90°), as predicted by theory. Computations of sin $(\eta_{un} - \eta_{vn})$ show that the semidiurnal harmonic wind turns clockwise with time at each range gate, with the exception of the lowest two range gates and the highest range gate.

Data for each of the four stations, from tables similar to Table 2, are plotted in composite figures to illustrate the key features of the semidiurnal harmonic. Figure 7 shows that the semidiurnal u- and v-component amplitudes are quite weak near the ground at all four sites but increase with height at HUD, PLT, and TBR to attain about 0.7 m s^{-1} at altitudes between 5000 and 7000 m MSL. This increase in semidiurnal amplitudes with height in the troposphere agrees with Wallace and Tadd's (1974) rawinsonde analyses. At HAV, however, the amplitudes appear to be rather

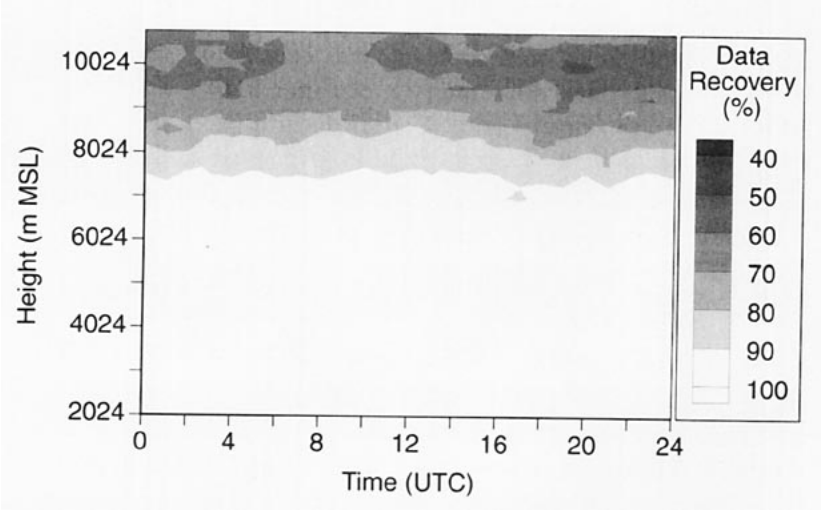

FIG. 6. Diurnal variations in the height of coverage of the 404-MHz profiler at Platteville, Colorado.

TABLE 2. Daily mean u and v wind components, amplitudes of the u and v wind components, times of the u and v wind component maxima, and normalized power densities for the diurnal and semidiurnal harmonics at PLT.

Height (m MSL)	u_0 (m s^{-1})	v_0 (m s^{-1})	A_{u1} (m s^{-1})	t_{u1} (LMST)	A_{v1} (m s^{-1})	t_{v1} (LMST)	A_{u2} (m s^{-1})	t_{u2} (LMST)	A_{v2} (m s^{-1})	t_{v2} (LMST)	P_1	P_2
2024	1.14	−0.80	0.53	3.26	0.34	15.90	0.15	8.93	0.29	2.18	0.61	0.16
2274	1.64	−1.58	0.50	3.51	0.27	16.26	0.14	10.37	0.18	0.85	0.62	0.10
2524	2.40	−2.07	0.33	3.63	0.34	21.07	0.12	0.15	0.26	11.66	0.47	0.17
2774	3.16	−2.67	0.11	6.86	0.67	21.09	0.11	1.92	0.34	11.99	0.64	0.18
3024	3.90	−3.26	0.26	12.80	0.88	20.98	0.23	3.77	0.46	0.52	0.71	0.22
3274	4.51	−3.89	0.49	14.39	0.76	20.85	0.49	3.53	0.39	0.59	0.63	0.30
3524	4.98	−4.37	0.62	15.36	0.74	20.66	0.57	3.66	0.46	0.38	0.59	0.34
3774	5.35	−4.71	0.67	15.76	0.63	20.66	0.61	3.58	0.45	11.97	0.55	0.37
4024	5.70	-5.09	0.72	15.55	0.52	20.95	0.66	3.74	0.39	0.33	0.53	0.40
4274	5.97	−5.40	0.73	15.10	0.38	21.36	0.64	4.03	0.40	0.53	0.48	0.41
4524	6.27	−5.68	0.65	15.03	0.25	23.07	0.50	4.21	0.47	0.87	0.45	0.44
4774	6.61	−5.84	0.63	14.91	0.21	0.19	0.59	4.22	0.55	0.92	0.37	0.54
5024	6.97	−5.92	0.73	14.97	0.23	0.51	0.64	4.35	0.65	0.75	0.39	0.56
5274	7.35	−5.92	0.67	14.93	0.25	0.85	0.61	4.51	0.62	0.68	0.37	0.56
5524	7.72	−5.92	0.54	14.66	0.21	0.74	0.60	4.68	0.58	0.66	0.30	0.62
5774	8.10	−5.91	0.48	14.33	0.24	0.64	0.55	4.44	0.64	0.83	0.27	0.65
6024	8.50	−5.80	0.44	13.44	0.28	0.66	0.50	4.55	0.68	0.86	0.24	0.63
6274	8.86	−5.70	0.45	12.54	0.37	23.27	0.59	4.24	0.74	1.20	0.24	0.64
6524	9.22	−5.58	0.49	12.29	0.40	23.06	0.66	3.99	0.72	1.17	0.25	0.59
6774	9.41	−5.28	0.43	11.92	0.31	0.48	0.73	4.02	0.78	1.17	0.17	0.69
7024	9.92	−5.12	0.49	11.48	0.26	2.70	0.77	3.81	0.68	0.65	0.17	0.57
7274	10.38	−4.85	0.36	11.67	0.51	4.12	0.82	3.96	0.79	1.43	0.18	0.59
7524	10.87	−4.69	0.53	11.23	0.68	4.99	0.68	4.01	0.61	1.13	0.39	0.44
7774	10.84	−4.57	0.53	10.74	0.50	6.29	0.25	5.90	0.65	0.87	0.31	0.29
8024	11.09	−4.24	0.72	9.95	0.81	7.95	0.35	4.67	0.88	0.37	0.39	0.30
8274	11.26	−3.93	0.44	8.86	1.12	8.61	0.29	6.29	0.77	11.28	0.43	0.20

constant with height, as predicted by Forbes's (1982) dynamic tidal model, although the amplitudes, especially for the v component, are somewhat stronger than the predictions of 0.1–0.2 m s^{-1}.

Figure 8 shows the phase of the semidiurnal oscillations represented in terms of the LMST of the u and v wind component maxima. Above the shallow wintertime boundary layers (i.e., the first few range gates), the times of the individual component maxima are quite consistent between sites—the u-component maxima occurs at about 0400 (and 1600), and the v-component maxima occurs at about 0100 (and 1300) LMST. The semidiurnal wind turns clockwise with time, and because the two semidiurnal components are 90° out of phase and of approximately equal amplitude, hodographs (Fig. 9) of the semidiurnal components are approximately circular. The amplitudes and phases of the semidiurnal wind components are similar at all four sites, despite the different locations of the stations and despite significant differences in the mean winds, a feature that is emphasized by the choice of coordinates in Fig. 9. When the phases are considered in terms of UTC rather than LMST, the semidiurnal wave is seen to be a traveling wave, which progresses around the earth following the sun's apparent motion.

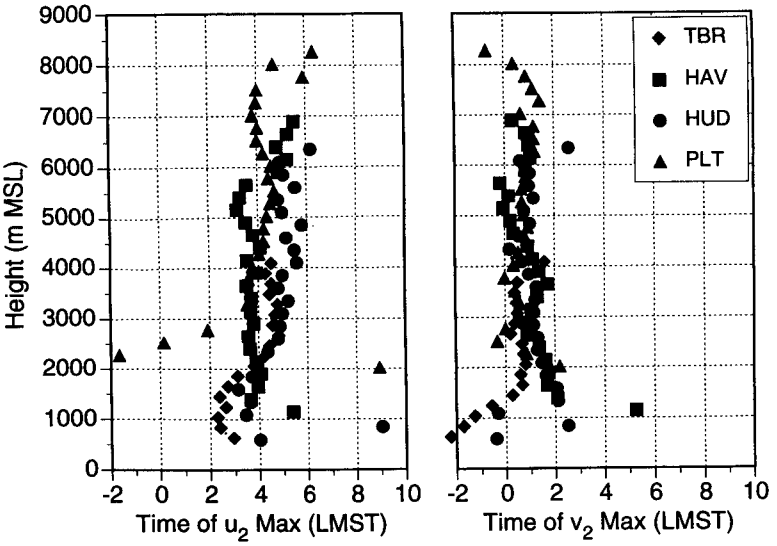

FIG. 7. Semidiurnal wind component amplitudes as a function of height.

5. Implicit filtering and error estimation

The vector averaging that is used to preprocess the radar profiler data provides an effective filter that allows the harmonic components (i.e., components of frequency 24/n hours, n = 1, 2, . . . , 12) to pass but filters all other oscillations, including synoptic wind oscillations. The longer the period of record, the more effective the filter. While there is a general agreement among the amplitudes and phases of the semidiurnal oscillations at the four stations, a key concern is the accuracy of their determination given the rather short period of record. If the accuracy is poor, then one cannot have confidence that the differences in tidal wind characteristics between stations such as those seen in Figs. 7 and 8, which might be produced, for example, by localized terrain–tidal interactions, are significant.

Statistical methods for determining error bars for harmonic amplitudes and phases were developed by Bartels (1932). His method has been summarized by Chapman and Lindzen (1970) and Craig (1965), among others, and requires that a long wind record be broken into smaller subrecords that are considered to be independent samples of the population. A measure of the deviation in amplitudes and phases associated with the independent samples, as plotted on a harmonic dial, defines the confidence

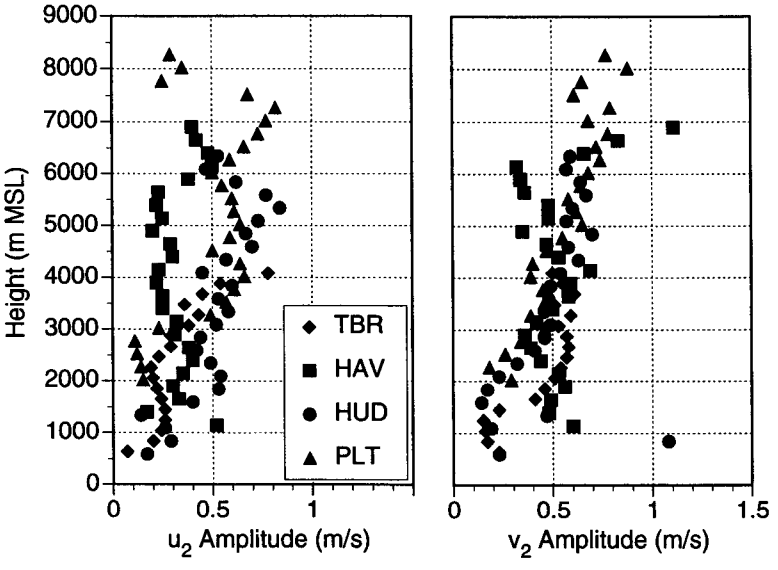

FIG. 8. Semidiurnal wind component phases as a function of height. Times are local mean solar time.

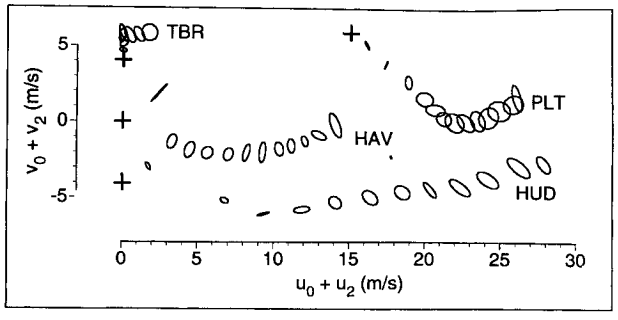

FIG. 9. Hodograms of the sum of the mean daily and mean hourly semidiurnal wind components at the four sites. Twenty-four hourly points make up the elliptical wind figures for each range gate. Each of the hourly points can be thought of as defining the tip of a wind vector drawn from the coordinate origin, indicated for each site by a plus sign. This vector rotates clockwise twice per day around each of the hodograms. For use, the u- and v-component scales must be shifted to the origin for each of the sites. The first range gates are at 2024, 593, 637, and 1148 m MSL for HAV, HUD, PLT, and TBR, respectively. Additional plotted range gates are at 500-m intervals for HAV, HUD, and PLT and at 406-m intervals for TBR, so that the highest plotted range gates are at 8024, 6093, 3885, and 6648 m MSL, respectively.

in the determination of the true mean of the population. In the present work, however, it proves infeasible to use Bartels's technique because about 30–45 days of data are required to obtain a realistic single determination of the amplitude and phase of the semidiurnal signal, and the number of such samples is severely limited by the total period of record (see Table 1).

An estimate of radar profiler tidal amplitude measurement errors can be obtained by assuming that tidal phase does not vary with height, that the time of the east (north) component maximum is 0344 (0044) LMST, and that the rotation of the semidiurnal wind vector is roughly circular. The first assumption, that tidal phase does not vary with height in the troposphere, is supported by both observational (Wallace and Tadd 1974) and modeling studies (Forbes 1982). The second assumption, regarding phases, is generally valid, although Spar (1952) has shown that tidal phases vary near seacoasts and, especially, to the west of major north–south mountain barriers. The third assumption is supported by Fig. 9. With these assumptions, the tidal amplitude error δA is related to measured phase deviations $\delta\eta$ by the equation $\delta A = A \sin \delta\eta$. We apply this equation to estimate general radar profiler amplitude errors for about three months of hourly data by considering the two sites HAV and PLT, which are not located near coastlines or on the western side of major mountain barriers. At HAV, the mean amplitude error for the altitude range 2148–5898 m MSL is 0.04 m s^{-1} for the u component and 0.12 m s^{-1} for the v component. Larger errors occur near the ground (0.09 m s^{-1} for the u component and 0.27 for v for the altitude range 1148–1898 m MSL) and at the top of the sounding (0.33 m s^{-1} for the u component and 0.15 m s^{-1} for v for the altitude range 6148–6898 m MSL). At PLT, the mean amplitude error (3024–8024 m MSL) is 0.12 m s^{-1} for the u component and 0.09 m s^{-1} for the v component, with larger errors occurring near the ground. These calculations suggest that, except for those range gates near the ground and at higher altitudes where data are missing, the radar profiler amplitude errors are generally between 0.1 and 0.2 m s^{-1}. If this rough error assessment proves accurate, radar profilers will be able to provide important information on the spatial variability of the atmospheric tides using a few years of records rather than decades.

6. Conclusions

The study of semidiurnal tides provides an interesting insight into the way in which the Earth's atmosphere responds to an extraterrestrial influence—namely, the input of solar energy and the local heating of the atmosphere by absorption in regions with strongly absorbing atmospheric constituents.

The most apparent effect of the semidiurnal tide at the earth's surface is a regular semidiurnal signal in surface pressures observed over the whole globe, but with strongest amplitude at the equator. A simple two-dimensional dynamical model of the atmosphere can predict the basic characteristics of the semidiurnal tidal wind system that must accompany these pressure perturbations. The key characteristics include the twice-daily cycle of tidal winds, their clockwise rotation with time, their distribution and propagation around the globe following the traveling pressure perturbation, their phase relationship with the semidiurnal pressure patterns, and their amplitude.

Pulsed Doppler radar wind profilers provide continuous records of wind profiles in the troposphere, averaged over hourly intervals and over fixed atmospheric volumes. Absolute accuracies of radar profiler wind speeds, for example, for 915-MHz profilers, have been reported to be about 1 m s^{-1} (Furger et al. 1995), and it is a surprising result that radar profilers can be used to observe the climatological signature of the small tropospheric tidal wind perturbation. This

is, no doubt, due to the strong filtering effects introduced by the compositing of radar profiler data into a climatological mean day before the harmonic analysis is done. This compositing provides an implicit bandpass filter, which passes the diurnal signal and its harmonics while filtering out longer and shorter period signals whose phases change from day to day. Thus, for example, traveling synoptic-scale disturbances are effectively filtered if the period of record is long enough to ensure that many such traveling disturbances transit past the profiler at varying times of day. The data from 915-, 404-, and 50-MHz profilers are suitable for the analysis of semidiurnal tidal wind systems in the troposphere, and when 30–45 days of wind data are available, a harmonic analysis of vector-averaged wind fields can detect the midlatitude semidiurnal tidal signal. The characteristics of the tidal wind system are quite distinctive in climatological analyses of such records. Our analyses of data from four locations covering a wide longitude zone in the United States show that the observed wind characteristics generally agree with predictions of the simple two-dimensional dynamical model described above.

Further information on tidal characteristics in the troposphere will come from longer-term records of wind profiles from UHF and VHF profilers distributed widely over the Earth's surface. The vertical structure of these tides in the troposphere is, at this time, not well known, and further data should provide important new knowledge on this characteristic of the tides. As the global spatial variations of tidal characteristics become better known and appropriate error bars can be attached to the amplitudes and phases, the effects of tidal–mountain interactions will become clearer, and it may also become possible to determine the relative roles of various atmospheric absorbers in producing the tides. Further research is necessary to determine the influence of the tidal wind oscillations on precipitation, cloudiness, and fogs.

Acknowledgments. The 404-MHz data were collected by NOAA Forecast Systems Laboratory's Wind Profiler Demonstration Network and were supplied by Dr. Ray Arritt of Iowa State University. The 915-MHz data were collected by NOAA's Environmental Technology Laboratory (ETL) as part of the 1992 MOHAVE Project. Dr. John Gaynor of ETL and Mr. Norm Robinson of Desert Research Institute supplied these data. Mr. Dan Wolfe of ETL is thanked for information on radar profiler operation, Dr. Jim Wilczak of ETL provided valuable advice on the analysis approach, and Dr. Ruedi Weber of the Paul Scherrer Institute is thanked for his statistical advice regarding error bar computations. Dr. Chris Williams of NOAA's Aeronomy Laboratory provided comments and advice regarding harmonic filters.

The paper was completed while one of the authors (C. David Whiteman) was on a short-term assignment in Switzerland at the Paul Scherrer Institute and at the Geographical Institute of the University of Bern. Dr. Markus Furger and Dr. Heinz Wanner are thanked for arranging these assignments, providing research facilities, and for the many kindnesses extended during the research appointments.

We thank the American Geophysical Union for their permission to reproduce some of the radar profiler analyses that we first reported in an article published in *Geophysics Research Letters.*

Research was supported by the U.S. Department of Energy (DOE) under Contract DE-AC06-76RLO 1830 at Pacific Northwest Laboratory as part of DOE's Atmospheric Studies in Complex Terrain and Atmospheric Radiation Measurements programs. Pacific Northwest Laboratory is operated for the DOE by Battelle Memorial Institute.

References

Bartels, J., 1932: Statistical methods for research on diurnal variations. *Terr. Magnet. Atmos. Elec.,* **37,** 291–302.

Brier, G. W., and J. Simpson, 1969: Tropical cloudiness and rainfall related to pressure and tidal variations. *Quart. J. Roy. Meteor. Soc.,* **95,** 120–147.

Butler, S. T., and K. A. Small, 1963: The excitation of atmospheric oscillations. *Proc. Roy. Soc. London,* **A274,** 91–121.

Chapman, S., 1918: The lunar atmospheric tide at Greenwich 1854–1917. *Quart. J. Roy. Meteor. Soc.,* **50,** 165–195.

——, 1951: Atmospheric tides and oscillations. *Compendium of Meteorology,* T. F. Malone, Ed., Amer. Meteor. Soc., 510–530.

——, and R. S. Lindzen, 1970: *Atmospheric Tides.* D. Reidel Publishing Co., 200 pp.

Craig, R. A., 1965: *The Upper Atmosphere: Meteorology and Physics.* International Geophysics Series, Vol. 8, Academic Press, 509 pp.

Davies, H. C., and P. D. Phillips, 1985: Mountain drag along the Gotthard section during ALPEX. *J. Atmos. Sci.,* **42,** 2093–2109.

Doviak, R. J., and D. S. Zrnic, 1993: *Doppler Radar and Weather Observations.* Academic Press, 562 pp.

Forbes, J. M., 1982: Atmospheric tides 2. The solar and lunar semidiurnal components. *J. Geophys. Res.,* **87,** 5241–5252.

——, and M. E. Hagan, 1988: Diurnal propagating tide in the presence of mean winds and dissipation: A numerical investigation. *Planet. Space Sci.,* **36,** 579–590.

Frei, C., 1994: Excitation and modification of geophysical boundary-related flow phenomena: Some modelling studies. Ph.D. dissertation, Swiss Federal Institute of Technology, 130 pp.

——, and H. C. Davies, 1993: Anomaly in the Alpine diurnal pressure signal: Observations and theory. *Quart. J. Roy. Meteor. Soc.,* **119,** 1269–1289.

Furger, M., C. D. Whiteman, and J. M. Wilczak, 1995: Uncertainty of boundary layer heat budgets computed from wind profiler–RASS networks. *Mon. Wea. Rev.,* **123,** 790–799.

Greenhow, J. S., and E. L. Neufeld, 1961: Winds in the upper atmosphere. *Quart. J. Roy. Meteor. Soc.*, **87,** 472–489.

Hamilton, K., 1981: A note on the observed diurnal and semidiurnal rainfall variations. *J. Geophys. Res.*, **86,** 12 122–12 126.

——, 1983: Quasi-biennial and other long period variations in the solar semidiurnal barometric oscillation: Observations, theory and possible application to the problem of monitoring changes in global ozone. *J. Atmos. Sci.*, **40,** 2432–2443.

——, 1984: Calculation of the effect of stratospheric mean wind variations on the solar semidiurnal barometric oscillation. *Atmos.–Ocean,* **22,** 48–66.

Haurwitz, B., 1956: The geographical distribution of the solar semidiurnal pressure oscillation. *N. Y. Univ. Coll. of Eng. Meteor. Pap.*, **2** (5), 1–36.

——, 1962: Wind and pressure oscillations in the upper atmosphere. *Arch. Meteor. Geophys. Bioklim.*, **13,** 144–165.

——, and A. D. Cowley, 1969: The lunar semidiurnal wind variations at Hongkong and Uppsala. *Quart. J. Roy. Meteor. Soc.*, **95,** 766–770.

——, and ——, 1970: The lunar barometric tide, its global distribution and annual variation. *Pure Appl. Geophys.*, **75,** 1–29.

Kelvin, Lord (Thompson, W.), 1882: On the thermodynamic acceleration of the earth's rotation. *Proc. Roy. Soc. Edinburgh,* **11,** 396–405.

Kertz, W., 1951: Theorie der gezeitenartigen Luftschwingungen als Eigenwertproblem (Theory of Time-Dependent Atmospheric Oscillations as an Eigenvalue Problem). *Ann. Meteorol.*, **4,** Suppl. 1, 1–31.

Laplace, P. S. (later Marquis de la Place), 1825: Mécanique Céleste. Livre 4, Chapitre 5, Paris.

Lindzen, R. S., 1967: Thermally driven diurnal tide in the atmosphere. *Quart. J. Roy. Meteor. Soc.*, **93,** 18–42.

——, 1978: Effect of daily variations of cumulonimbus activity on the atmospheric semidiurnal tide. *Mon. Wea. Rev.*, **106,** 526–533.

——, 1979: Atmospheric Tides. *Ann. Rev. Earth Planet. Sci.*, **7,** 199–225.

——, 1990: *Dynamics in Atmospheric Physics.* Cambridge University Press, 310 pp.

——, and S. S. Hong, 1974: Effects of mean winds and horizontal temperature gradients on solar and lunar semidiurnal tides in the atmosphere. *J. Atmos. Sci.*, **31,** 1421–1446.

Neff, W. D., 1990: Remote sensing of atmospheric processes over complex terrain. *Atmospheric Processes over Complex Terrain,* Meteor. Monogr., No. 45, Amer. Meteor. Soc., 173–228.

Newton, I., 1687: *Philosophiae Naturalis Principia Mathematica.*

Siebert, M., 1961: Atmospheric tides. *Advances in Geophysics,* Vol. 7, Academic Press, 105–187.

Spar, J., 1952: Characteristics of the semidiurnal pressure waves in the United States. *Bull. Amer. Meteor. Soc.*, **33,** 438–441.

Strauch, R. G., D. A. Merritt, K. P. Moran, K. B. Earnshaw, and D. van de Kamp, 1984: The Colorado wind profiling network. *J. Atmos. Oceanic Technol.*, **1,** 37–49.

Stull, R. B., 1988: *An Introduction to Boundary Layer Meteorology.* Kluwer Academic Publishers, 666 pp.

U.S. Dept. of Comerce, Weather Bureau, 1943: 10-year normals of pressure tendencies and hourly station pressures for the United States. U.S. Weather Bureau Tech. Paper No. 1, 79 pp.

Wallace, J. M., 1975: Diurnal variations in precipitation and thunderstorm frequency over the conterminous United States. *Mon. Wea. Rev.*, **103,** 406–419.

——, and F. R. Hartranft, 1969: Diurnal wind variations, surface to 30 kilometers. *Mon. Wea. Rev.*, **97,** 446–455.

——, and R. F. Tadd, 1974: Some further results concerning the vertical structure of atmospheric tidal motions within the lowest 30 kilometers. *Mon. Wea. Rev.*, **102,** 795–803.

Walterscheid, R. I., and J. G. DeVore, 1981: The semidiurnal atmospheric tide at the equinoxes: A spectral study with mean-wind-related influences and improved heating rates. *J. Atmos. Sci.*, **38,** 2291–2304.

Whiteman, C. D., and X. Bian, 1994: Semidiurnal solar tides in the mountain atmosphere. *Ann. Meteor.*, **30,** 239–242.

——, and ——, 1995: Radar wind profiler observations of solar semidiurnal atmospheric tides. *Geophys. Res. Lett.*, **22,** 901–904.

Wilczak, J. M., and Coauthors, 1995: Contamination of wind profiler data by migrating birds: Characteristics of corrupted data and potential solutions. *J. Atmos. Oceanic Technol.*, **12,** 449–467.

Williams, C. R., S. K. Avery, J. R. McAfee, and K. S. Gage, 1992: Comparison of observed diurnal and semidiurnal tropospheric winds at Christmas Island with tidal theory. *Geophys. Res. Lett.*, **19,** 1471–1474.

Zwiers, F., and K. Hamilton, 1986: Simulation of solar tides in the Canadian Climate Center general circulation model. *J. Geophys. Res.*, **91,** 11 877–11 896.